Environmental Science Processes & Impacts

ROYAL SOCIETY OF CHEMISTRY

PAPER

View Article Online
View Journal | View Issue

Cite this: *Environ. Sci.: Processes Impacts*, 2025, **27**, 2821

Overcoming the challenge of quantifying aged microplastic by qNMR spectroscopy

Julia Schmidt, *[a] Marte Haave [c] and Wei Wang [ab]

Quantitative nuclear magnetic resonance (qNMR) spectroscopy holds strong potential for environmental microplastic analysis, contingent on addressing the challenge of quantifying aged synthetic microplastics. This study evaluated the application of qNMR for quantifying polystyrene (PS), polyvinyl chloride (PVC), and polyethylene terephthalate (PET), aged under UV exposure and elevated temperatures for 24 days. qNMR was combined with scanning electron microscopy (SEM) and Fourier-transform infrared (FTIR) spectroscopy to assess morphological, chemical, and molecular-level changes. SEM revealed surface degradation in PS and PVC, with minimal changes in PET, while FTIR showed increased carbonyl indices (CI), indicating oxidation. qNMR analysis demonstrated consistent microplastic signals between aged and pristine materials, with relative quantification errors from 1% to 18%. Calibration curves showed strong linearity (R^2 > 0.97), with limits of detection (LOD) between 0.87–2.79 μg mL^{-1} and limits of quantification (LOQ) between 2.89–9.29 μg mL^{-1}. Additionally, degradation products in PS and PVC were quantified, providing a detailed assessment of chemical changes during aging, while PET exhibited no significant degradation. These results demonstrate that qNMR enables sensitive, reliable quantification of aged microplastics. Integration of qNMR, SEM, and FTIR offers complementary insights into microplastic aging and supports the development of robust methods for environmental microplastic monitoring.

Received 23rd May 2025
Accepted 7th August 2025

DOI: 10.1039/d5em00393h

rsc.li/espi

Environmental significance

Accurate quantification of microplastics, particularly in their aged and environmentally degraded forms, remains a major analytical barrier in understanding their fate and impact. This study demonstrates the application of quantitative nuclear magnetic resonance (qNMR) spectroscopy, supported by SEM and FTIR, as a robust and sensitive approach for characterizing and quantifying aged synthetic microplastics, including PS, PVC, and PET. By establishing reliable calibration and detection limits for these weathered particles, the work advances analytical capabilities for mass-based microplastic assessment. This methodological development contributes to improving the traceability and risk assessment of weathered microplastics, supporting more effective environmental monitoring and regulation.

Introduction

Microplastic (MP; 1 μm to 5 mm)[1–4] and nanoplastic (NP; <1 μm)[5–11] pollution has become a global concern due to their widespread occurrence and the potential risks they pose to ecosystems and human health.[12–15] MPs primarily originate from the environmental degradation of larger plastic debris, driven by ultraviolet (UV) radiation, temperature fluctuations, mechanical stress, and oxidative conditions.[16–21] Despite the addition of plasticizers, antioxidants, and stabilizers during production to enhance the durability of plastics in their intended applications,[16–18,22,23] aging leads to fragmentation into MPs and NPs. These degradation processes cause surface cracking, porosity, and chemical alterations within the MP matrix.[19–21,24] Oxidative degradation introduced oxygen-containing functional groups such as carboxylic acids, aldehydes, ketones, and hydroxyls,[25,26] which increase the polarity and, consequently, the hydrophilicity of MPs while reducing their hydrophobicity.[27] As a result, aged MPs more readily absorb environmental pollutants including hydrophobic organic compounds, antibiotics, and metal ions.[25,28] These alterations have been linked to toxicological effects, including cancer, reproductive disorders and cardiovascular disease.[29–32] Photochemical degradation, especially from UV exposure, is a major driver of these changes, inducing polymer chain scission, free radical generation, and oxidation.[15,33–38] Prolonged exposure intensifies these effects, altering particle morphology and molecular weight distribution.[39] Fourier-transform infrared (FTIR) spectroscopy is commonly used to characterize these changes, identifying shifts in functional groups and enabling weathering indices like the carbonyl index (CI) to assess degradation extent.[25,40–42] However,

[a]*Department of Chemistry, University of Bergen, 5007 Bergen, Norway. E-mail: Julia.Schmidt@uib.no*
[b]*Centre for Pharmacy, University of Bergen, 5020 Bergen, Norway*
[c]*SALT Lofoten AS, 8301 Svolvær, Norway*

FTIR and scanning electron microscopy (SEM) mainly provide surface-level information and lack molecular-level resolution. To investigate deeper structural and compositional changes, nuclear magnetic resonance (NMR) spectroscopy, particularly proton (^{1}H) and quantitative NMR (qNMR), offers a promising analytical alternative. NMR has been applied to a wide range of MPs, including low-density polyethylene (LDPE), polystyrene (PS), polyethylene terephthalate (PET), acrylonitrile-butadiene-styrene (ABS), polyamide (PA), polyvinyl chloride (PVC), polyurethane (PU), polylactic acid (PLA), polybutadiene (PB), polyisoprene (PI), polymethyl methacrylate (PMMA), and polyacrylonitrile (PAN).[43–47] Both pure MPs and mixtures have been investigated, demonstrating the capability of NMR to analyse overlapping proton signals in complex matrices.[48,49] Techniques such as 2D ^{1}H diffusion-ordered spectroscopy,[50] low-field ^{1}H NMR,[51] and ^{13}C multi-cross-polarization[52] have also shown promise.

Although ^{1}H NMR has been applied to assess accelerated aged MPs,[53] the use of qNMR to quantify aged MPs, particularly in environmentally relevant samples, remains underexplored. This study aims to fill this gap by evaluating the effectiveness of qNMR in quantifying MPs aged through UV exposure and elevated temperature. Additionally, the study investigated the limit of detection (LOD) and limit of quantification (LOQ) for these aged MPs, assessing the sensitivity and applicability of qNMR. By combining qNMR with SEM and FTIR, this study explores whether qNMR can reliably identify and quantify morphologically and chemically altered MPs. This study takes a critical step toward evaluating the feasibility and limitations of qNMR spectroscopy for analysing complex, aged environmental MPs, forming the basis for cost-effective monitoring of both new and weathered MPs (Schmidt *et al.*, in prep).

Experimental

Materials

PS beads (900 μm), PET powder (300 μm) from GoodFellow Cambridge Ltd, England, and PVC powder (<50 μm) from Werth-Metall, Germany, were used as model MPs. Deuterated solvents, including tetrahydrofuran (THF-d_8, ≥99.5 atom% D; residual proton signals at 3.58 ppm and 1.73 ppm) purchased from VWR International, LLC, deuterated chloroform ($CDCl_3$, 99.8 atom% D; residual proton signal at 7.26 ppm), and deuterated trifluoroacetic acid (TFA-d, >99.5 atom% D; residual proton signal at 11.50 ppm), both from Sigma-Aldrich®, were used in this study. Dimethyl sulfone ($DMSO_2$), purchased from Sigma-Aldrich®, TraceCERT®, with its residual proton signal at 3.00 ppm, was used as the internal standard.

Sample preparation

Accelerated aging the of MPs. For the artificial aging process, 1–2 g each of MP sample (PS, PVC and PET) were evenly distributed on separate glass Petri dishes and placed in a laboratory oven maintained at a constant temperature of 50 °C to accelerate the aging process. Additionally, a UV lamp (ENF-280C/FE from Spectroline®) emitting shortwave light at 254 nm with an intensity of 450 μW cm^{-2} at a distance of 15 cm was positioned directly on top of the Petri dishes. A 24-day aging process combining UV exposure and elevated temperature was applied to the MPs using a laboratory oven. To ensure an even aging, each Petri dish was carefully shaken every 24 hours. Samples were taken every second day and named according to the number of days aging, such as 0 d, 6 d, 12 d, 18 d, and 24 d.

Analysis by SEM, FTIR and carbonyl index. For the SEM images, samples from 0 d, 12 d, and 24 d were transferred and fixed onto individual SEM aluminium stubs using carbon adhesive tape. The samples were then coated with a thin layer of gold and palladium under vacuum conditions. All SEM images were captured using the ZEISS SUPRA 55VP field emission under high vacuum conditions, with a 5 kV beam voltage (EHT) and a working distance (WD) ranging from 5.3 to 6.2 mm. Images were taken at two different magnifications to capture the surface morphology comprehensively.

For the FTIR, replicate spectra and images of samples from pristine MPs as well as aged samples were collected on each sampling day as previously described. Measurements were performed using a Nicolet iS50 spectrometer (Thermo Fisher Scientific) equipped with a diamond ATR and an MCT/A detector, across the wavenumber range of 400 to 4000 cm^{-1} at a resolution of 4 cm^{-1}. The samples were loaded onto the diamond ATR platform and secured with pressure. Prior to initial sampling, a background spectrum was collected. The diamond sample platform was cleaned with methanol between each MP sample measurement. Each MP sample underwent 32 scans. The spectra were then processed using OMNIC software (version 9.8.286) from Thermo Fisher Scientific. From the obtained spectra, the CI, which is a measure of the degradation of MPs,[42] was calculated by determining the ratio of the integrated peak height of the carbonyl peaks to the integrated peak height of a stable reference peak for each spectrum.

Analysis by qNMR. For the qNMR analysis, PS and PVC were dissolved in THF-d_8, while PET was dissolved in a mixture of $CDCl_3$ and TFA-d (4 : 1), all at room temperature, with a nominal concentration of 1 mg mL^{-1}. The MP concentrations were analysed using $DMSO_2$ with a known concentration as an internal standard. For the NMR analysis, 600 μL of each sample solution was transferred into 5 mm NMR tubes (Bruker BioSpin, 4″ NMR tubes) for subsequent analysis. qNMR analysis was performed on all MP samples from 0 d, 12 d, and 24 d. To evaluate LOD and LOQ of the 24-day aged MPs, a calibration curve with six measuring points was utilized. Concentrations ranged from 0.5 to 10 μg mL^{-1} for PS and PVC in THF-d_8, and from 0.2 to 5 μg mL^{-1} for PET in $CDCl_3$/TFA-d (4 : 1). These concentration ranges were derived from the signal-to-noise (SNR)-based LOD and LOQ results for PS and PVC, as well as the relative response factor (RRF) approach for PET, which utilized LOD and LOQ data for PLA, as reported in our previous study.[46]

A Bruker Ascend 600 MHz spectrometer equipped with a QCI-P CryoProbe™ and an AVANCE NEO console, was used to conduct all NMR measurements at room temperature (298 K). The qNMR experimental parameters were consistent across all MP samples, with the pulse width and receiver gain

automatically optimized for each individual sample. Specifically, the spectral width was set to 29.76 ppm, 8 scans were acquired, the spectral size was 262 144 points, the acquisition time was 3.67 s, and a 60 s delay was used for each measurement.

The ^{1}H NMR spectra were visualized by importing the data into the NMR software program MestReNova (v14.2.0), while the qNMR spectra used for quantification were imported into Bruker's TopSpin NMR software (version 4.3.0). Manual phase and baseline correction were applied to all qNMR data, along with a line broadening of 0.1 Hz. A consistent ppm range was manually integrated across all samples for each MP type. To minimize potential measurement or integration errors, the internal standard method was used for quantitative analysis of the MPs,[54] with $DMSO_2$ serving as the internal standard in all samples, as previously published. The number of contributing nuclei was accounted for in the calculation of analyte concentrations. Full methodological details, including signal assignment and integration strategy, are described in our previous publication.[46] To support the assignment of degradation products, 2D NMR experiments (COSY, HSQC, and HMBC) were conducted on selected aged MP samples; experimental details and spectra are provided in the SI.

Calculations and statistical analysis

Statistical analyses and visualizations of CI data across the aging period were conducted using RStudio (version 4.3.0). A Langmuir adsorption model was applied to PS data, whereas linear regression models were used for PVC and PET. Additionally, LOD and LOQ for each MP after 24 days of aging were calculated based on the slope of the calibration curve (σ) and the standard deviation of the response (S), as described in eqn (1). The calibration curve was plotted as nominal concentration against the normalized integral. Model fit was evaluated using the coefficient of determination (R^2) values, with $R^2 > 0.99$ considered linear. A significance level of $p < 0.05$ was applied, and F-statistic tests were performed. Plots included 95% confidence intervals as upper and lower bounds.

$$\mathrm{LOD} = \frac{(3 \times \sigma)}{S} \quad \text{and} \quad \mathrm{LOQ} = \frac{(10 \times \sigma)}{S} \tag{1}$$

Furthermore, the relative error, representing the deviation between nominal (C_{nominal}) and measured (C_{measured}) MP concentrations, was calculated as described in eqn (2), with 0% indicating a perfect match.

$$\text{Relative error } [\%] = \frac{|C_{\mathrm{nominal}} - C_{\mathrm{measured}}|}{C_{\mathrm{nominal}}} \times 100 \tag{2}$$

Prevention of contamination and quality control

To reduce the potential for airborne MP contamination, glassware and other non-plastic equipment were thoroughly cleaned using distilled water and acetone. Prior to utilization, all glass flasks were dried at 60 °C for 24 hours in a closed and clean heating cabinet and subsequently sealed upon cooling. NMR tubes were dried at 60 °C for 30 minutes in a closet laboratory oven that had been cleaned with filtered 95% ethanol before use. Additional precautions were implemented, including the use of pure cotton lab coats to prevent contamination from clothing fibers and regular changes of nitrile gloves to prevent cross-contamination of MPs. Blanks were obtained by acquiring both ^{1}H NMR and qNMR spectra of pure THF-d_8 and $CDCl_3$/TFA-d (4 : 1) in the absence of any MP.

Results and discussion

SEM and FTIR signals change with MP aging

SEM images of pristine and aged MPs (PS, PVC, and PET) at two different magnifications (Fig. 1A–F, 2A–F and 3A–F) depict the morphological changes associated with the accelerated aging. The images show a progressive colour change during the aging, with samples transitioning from white (0 d) to yellow (12 d and 24 d), accompanied by increasing colour intensity. This color change indicates surface morphology changes in the MPs, mainly due to the degradation of unsaturated chromophoric groups upon UV irradiation.[55] Morphological changes were observed across all MPs during aging. The surface of pristine PS already exhibited visible microcracks and pores. Upon aging, these features became more defined and slightly enlarged, indicating progressive but subtle surface degradation. Notably, the overall surface texture appeared smoother in the aged samples, which may reflect partial melting or surface reflow effects included by the aging process. Previous studies observed microcracks, yellowing, and surface wrinkling after exposure to UV light (354 nm, 30 mW cm^{-2}), in some cases combined with elevated temperatures (50 °C), for exposures ranging from 96 hours to 30 days.[56–58] These results support the progressive, albeit moderate, morphological changes observed in the aged PS from this study.

In contrast, the spherical fine and coarse PVC grains, which form spherical agglomerates,[59,60] remained mostly intact during aging. Minimal surface structural changes may result from the shedding of the PVC skin, exposing the inner grains to further aging. Additionally, thermal degradation studies at 50 °C and 100 °C, conducted over an exposure period of 120 to 360 days, revealed that the surface of PVC appeared to have melted.[59] These changes could lead to embrittlement and disintegration during the degradation process.[34] Moreover, minimal morphological changes between pristine and aged samples of irregularly shaped and large PET fragments were observed; however, the surface of the aged PET appeared smoother. This lack of significant changes in PET could be attributed to its greater resistance to UV-induced degradation.[61]

FTIR analysis of PS, PVC and PET throughout the aging revealed distinct signs of their chemical transformations. In the case of pristine PS, the absorption bands corresponding to the hydroxyl (–OH) stretching vibrations in the range of 3600–3200 cm^{-1} and the carbonyl (–C=O) stretching at 1737.55 cm^{-1} were initially observed to be relatively weak (Fig. 1G).[62] However, with prolonged aging, FTIR showed a gradual increase in transmittance indicating the formation of functional groups on the PS surfaces. The CI of each sampling day was calculated

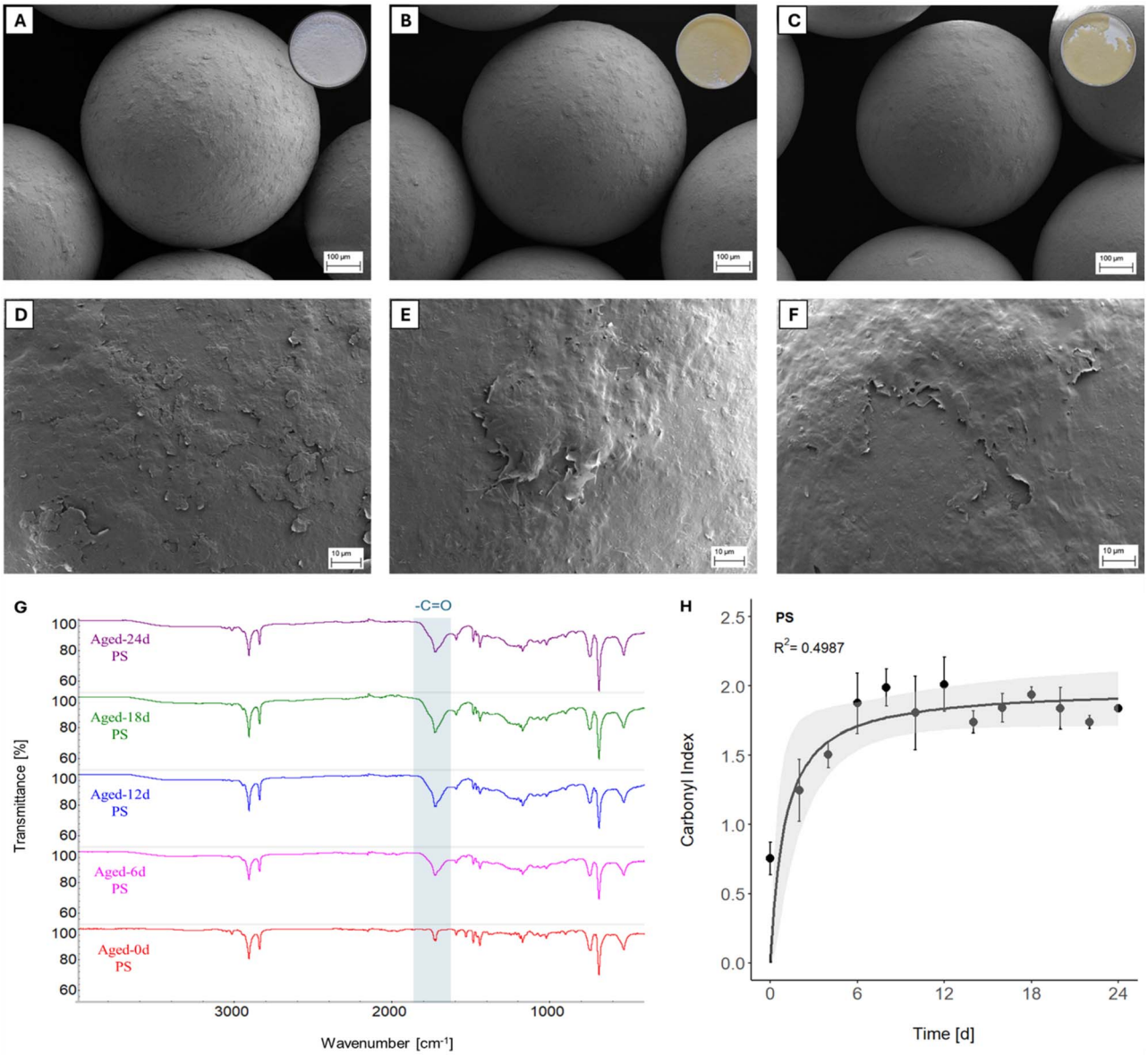

Fig. 1 SEM images of PS aged for (A and D) 0 days, (B and E) 12 days and (C and F) 24 days at two different magnifications, with corresponding photographs of the samples in Petri dishes displaying the colour change; (G) FTIR spectra of PS at five aging points; and (H) the CI plotted against time for all aging points, with error bars indicating the standard deviation of replicate measurements.

using the integrated peak heights of the carbonyl peak at 1735.55 cm^{-1} (using a baseline from 1899.54 cm^{-1} to 1639.19 cm^{-1}) and the stable reference peak at 2852.20 cm^{-1} (using a baseline from 2867.63 cm^{-1} to 2819.42 cm^{-1}) (Fig. 1G), and plotted against time, revealing a curved progression (Fig. 1H). To capture this nonlinear trend, a Langmuir adsorption model was applied to the CI data, yielding a pseudo-R^2 value of 0.4967 (*cf.* the SI). After day 6, the CI measured by FTIR levels off, indicating a stabilization in the FTIR response and suggesting minimal progression of aging-related chemical changes beyond this point.

Similarly, in pristine PVC, the absorption bands associated with hydroxyl (–OH) stretching vibrations in the 3600–3200 cm^{-1} region and carbonyl (–C=O) stretching at 1725.98 cm^{-1} were initially weak (Fig. 2G).[63] The CI was determined at five measurement points using the integrated peak heights of the carbonyl peak at 1725.98 cm^{-1} (using a baseline from 1874.47 cm^{-1} to 1535.42 cm^{-1}) and the stable reference peak at 1430.92 cm^{-1} (using a baseline from 1486.85 cm^{-1} to 1396.21 cm^{-1}) (Fig. 2G). The FTIR revealed a steady increase in CI with aging, implying a rise in surface functional groups for PVC. Moreover, the emergence of carbonyl and hydroxyl groups indicates that the aged PVC underwent oxidation reactions.[64] These chemical changes led to the formation of new functional groups, resulting in altered hydrophilicity of the MP.[24,64] The CI, plotted against time (Fig. 2H), shows a consistent and proportional increase, reflecting the progressive formation of carbonyl groups in PVC during the aging. The steady rise demonstrates

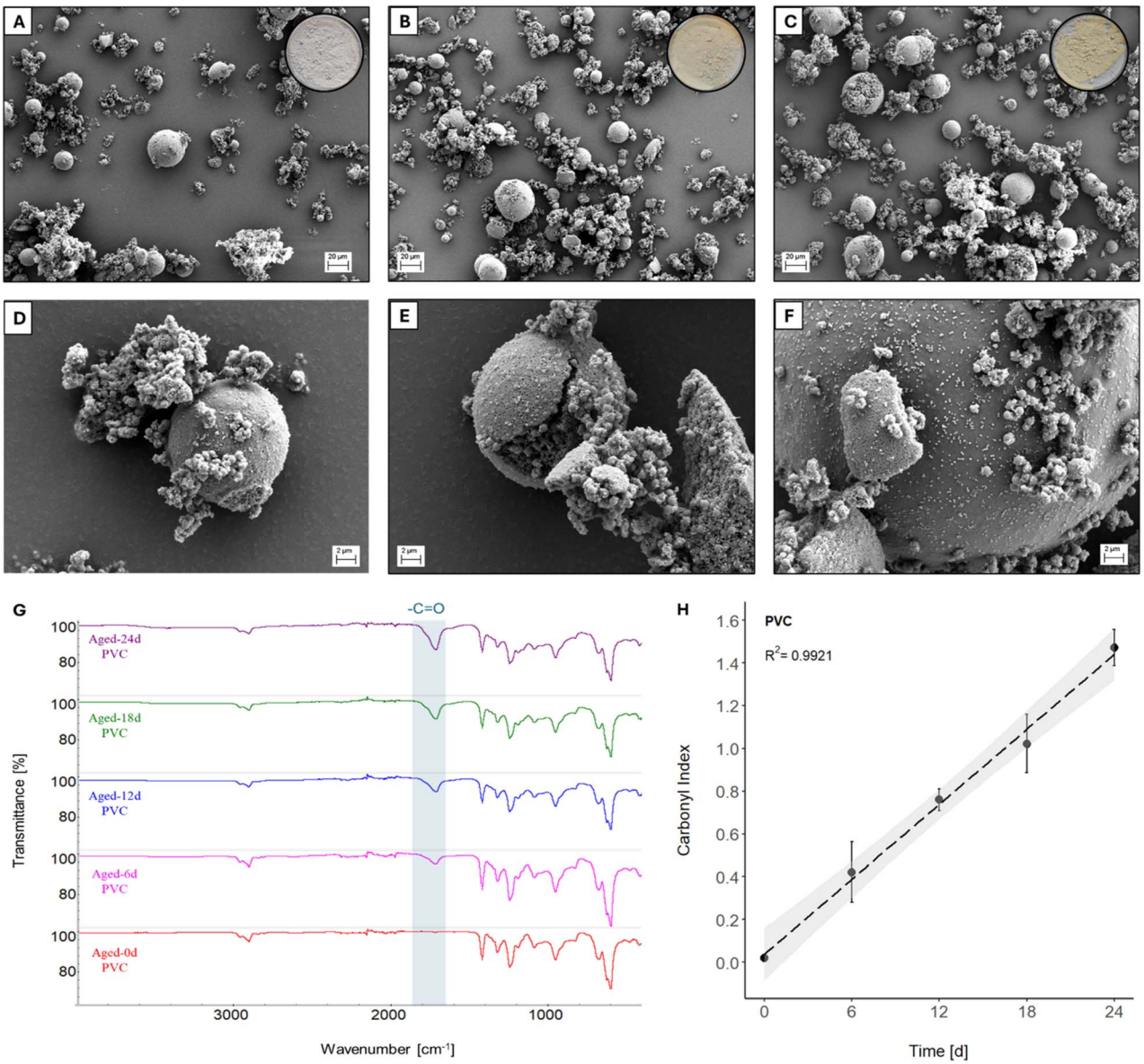

Fig. 2 SEM images of PVC aged for (A and D), 0 days, (B and E) 12 days and (C and F) 24 days at two different magnifications, with corresponding photographs of the samples in Petri dishes displaying the colour change; (G) FTIR spectra of PVC at five aging points; and (H) the CI plotted against time for the five aging points, with error bars indicating the standard deviation of replicate measurements.

that PVC oxidation follows a continuous and accumulating process, typical of photo-oxidative degradation, with surface modifications becoming more pronounced over time due to prolonged exposure to environmental stressors.[65] The linear regression with R^2 of 0.9921 (*cf.* the SI) further confirms this degradation trend, suggesting that the CI can track the aging state of PVC under both laboratory and environmental conditions.

In contrast, the absorption bands corresponding to the carbonyl (–C═O) stretching at 1717.41 cm^{-1} and the hydroxyl (–OH) stretching in the 3600–3200 cm^{-1} region,[66] remained relatively stable in PET (Fig. 3G). The CI showed minimal changes with aging, calculated at five measuring points using the integrated peak height of the carbonyl group at 1714.41 cm^{-1} (using a baseline from 1816.62 cm^{-1} to 1621.84 cm^{-1}) and the integrated peak height of the stable reference peak at 1241.93 cm^{-1} (using a baseline from 1324.86 cm^{-1} to 1182.15 cm^{-1}) (Fig. 3G). The CI was plotted against time (Fig. 3H), and a linear regression was used to fit the data, showing a steady but limited increase over time with an R^2 value of 0.9651 (*cf.* the SI). Since PET degradation is primarily driven by hydrolysis, which requires moisture, alcohol, and elevated temperatures to break ester bonds in the MP backbone,[67,68] the minimal changes observed in the CI indicate that significant degradation did not occur under the conditions used. These findings highlight that PET typically requires more extreme conditions, such as prolonged exposure or higher temperatures for significant degradation.[61] Overall, compared

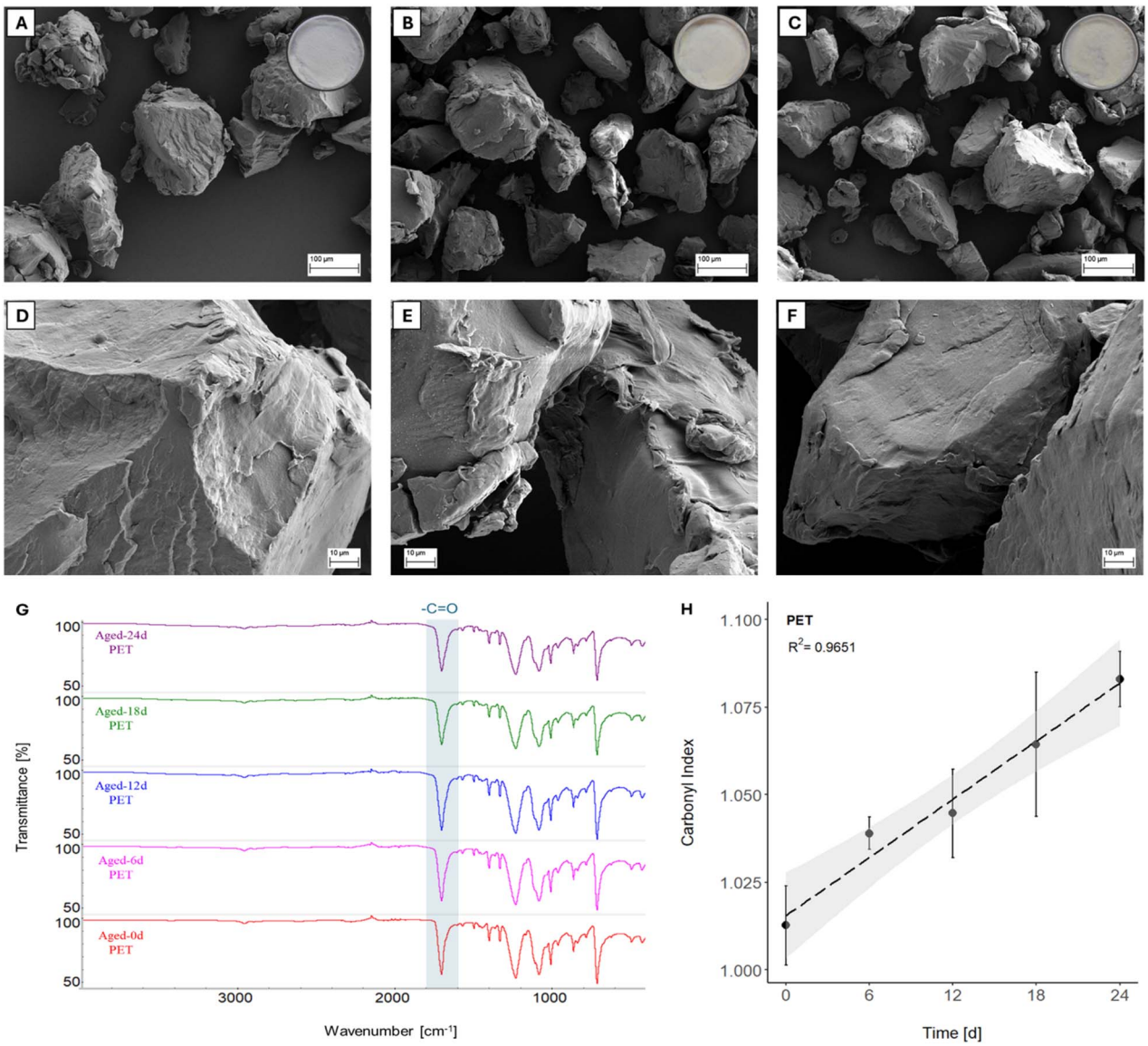

Fig. 3 SEM images of PET aged for (A and D) 0 days, (B and E) 12 days and (C and F) 24 days at two different magnifications, with corresponding photographs of the samples in Petri dishes displaying the colour change; (G) FTIR spectra of PVC at five aging points; and (H) the CI plotted against time for the five aging points, with error bars indicating the standard deviation of replicate measurements.

to PS, PVC exhibited a substantially greater increase in CI, approximately 69-fold, indicating more significant surface aging under UV radiation. When compared to PET, the increase in CI for PVC was nearly 100-fold greater.

Effectiveness of qNMR in quantifying aged MPs

The qNMR analysis was conducted to assess whether qNMR could correctly quantify the nominal concentrations of pristine as well as aged MPs (PS, PVC and PET). Proton signals of each MP were identified and assigned at distinct chemical shifts (Fig. 4). PS showed a proton signal in the range of 7.2 to 6.2 ppm, corresponding to the protons of the aromatic ring (H_a,H_b), PVC revealed a proton signal in the range of 4.73 to 4.28 ppm, corresponding to a CH group (H_a),[43,44,46] and PET showed proton signals at 8.12 ppm and 4.79 ppm, corresponding to the protons of the aromatic ring (H_a) and two CH_2 groups (H_b), respectively.[43] The full assigned ^{1}H NMR spectra of each MP can be found in Fig. S1–S3 in the SI.

A comparison of the proton signals from pristine and aged PS, PVC, and PET revealed no changes in the spectral shape of the specific proton signals previously assigned (Fig. 4). These specific proton signals were used for the quantitative analysis, and their consistency across both pristine and aged samples indicates that the aging process did not significantly affect their NMR spectra. This confirms that these key proton signals can be reliably detected and used to quantify the MPs by NMR spectroscopy, regardless of aging. Furthermore, the quantitative analysis demonstrated that the measured concentrations of both pristine and aged MPs closely matched the nominal values, with relative errors, calculated using eqn (2), ranging

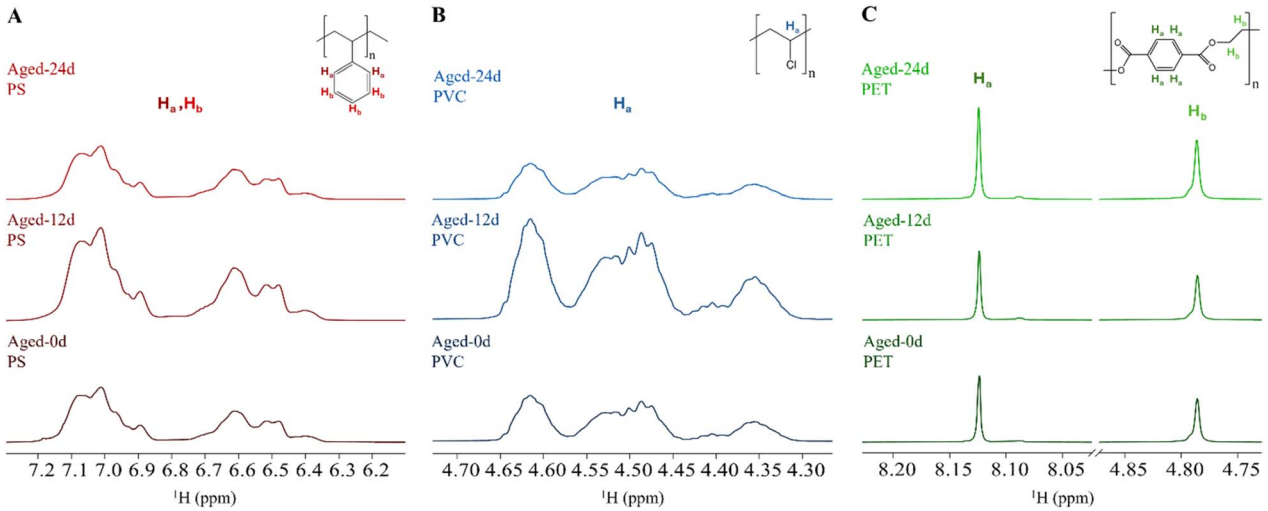

Fig. 4 ^{1}H NMR spectrum and structural formula of (A) PS and (B) PVC in THF-d_8 and (C) PET in $CDCl_3$/TFA-d (4 : 1) after 0 days, 12 days and 24 days of aging.

Table 1 Quantification of MP concentrations for PS and PVC in THF-d_8, and PET in $CDCl_3$/TFA-d (4 : 1), after 0 days, 12 days and 24 days of aging, with a nominal concentration of 1 mg mL^{-1}. Measured concentrations ($C_{measured}$), determined using the internal standard method with $DMSO_2$, along with the relative error (RE) are given for each MP

	PS		PVC		PET			
	H_a,H_b		H_a		H_a		H_b	
	$C_{measured}$ [mg mL^{-1}]	RE [%]	$C_{measured}$ [mg mL^{-1}]	RE [%]	$C_{measured}$ [mg mL^{-1}]	RE [%]	$C_{measured}$ [mg mL^{-1}]	RE [%]
0 d aged	0.99	1	1.08	8	1.00	0	1.05	5
12 d aged	1.18	18	1.15	15	0.99	1	1.04	4
24 d aged	0.97	3	0.93	7	1.10	20	1.13	13

from 1% to 18% (Table 1). These small deviations further validate the reliability and consistency of qNMR for MP quantification throughout the aging process. Although not formally validated for precision or reproducibility in this study, the consistent agreement between nominal and measured concentrations across aging stages, together with prior validation on pristine MPs[46] and polymer mixtures,[49] suggests that the qNMR approach is robust and reliable for quantifying aged MPs.

Calibration data for PS, PVC, and PET after 24 days of aging demonstrated strong linearity within their respective concentration ranges (Fig. 5). To support this, representative ^{1}H NMR spectra of the lowest and highest calibration points for each MP are included in Fig. S4 in the SI, illustrating the integration quality at the LOQ levels. For PS-H_a,H_b and PVC-H_a, calibration curves yielded R^2 values of 0.9976 and 0.9932, respectively. PET showed slightly lower but acceptable linearity, with R^2 values of 0.9752 and 0.9794 for the H_a and H_b proton signals, respectively. All LOD and LOQ values discussed below, both from the present study and prior literature, are based on qNMR methodologies, using either SNR criteria or internal standard approaches, unless otherwise stated. LOD and LOQ for PS were determined to be 1.10 μg mL^{-1} and 3.67 μg mL^{-1}, respectively (Table 2). These results are consistent with, and in some cases, more sensitive than those reported in previous studies on pristine MPs. For example, SNR-based LOD and LOQ values for PS have been reported at 2 μg mL^{-1} and >10 μg mL^{-1}, respectively, while internal standard-based LOQ was approximately 4 μg mL^{-1}.[46] The LOQ determined in this study is comparable to previously reported values, yet indicates that aged PS may be detected and quantified with marginally higher sensitivity than pristine PS. In contrast, another study reported substantially higher values for PS, with an LOD of 12 μg mL^{-1} and an LOQ of 77 μg mL^{-1},[43] highlighting the enhanced performance of the current method.

PVC exhibited higher LOD and LOQ values than PS, with 1.87 μg mL^{-1} and 6.22 μg mL^{-1}, respectively (Table 2). These values are also consistent with, or lower than, those previously reported for pristine PVC. Earlier studies noted an SNR-based LOD and of 1 μg mL^{-1} and an LOQ exceeding 10 μg mL^{-1}, along with an internal standard-based LOQ of 8 μg mL^{-1}.[46] These findings suggest that the quantification of aged PVC using qNMR remains comparable to, or even slightly more sensitive than, measurements of pristine PVC. Notably, previous studies reported considerably higher values with an LOD of 84 μg mL^{-1} and an LOQ of 281 μg mL^{-1},[44] further

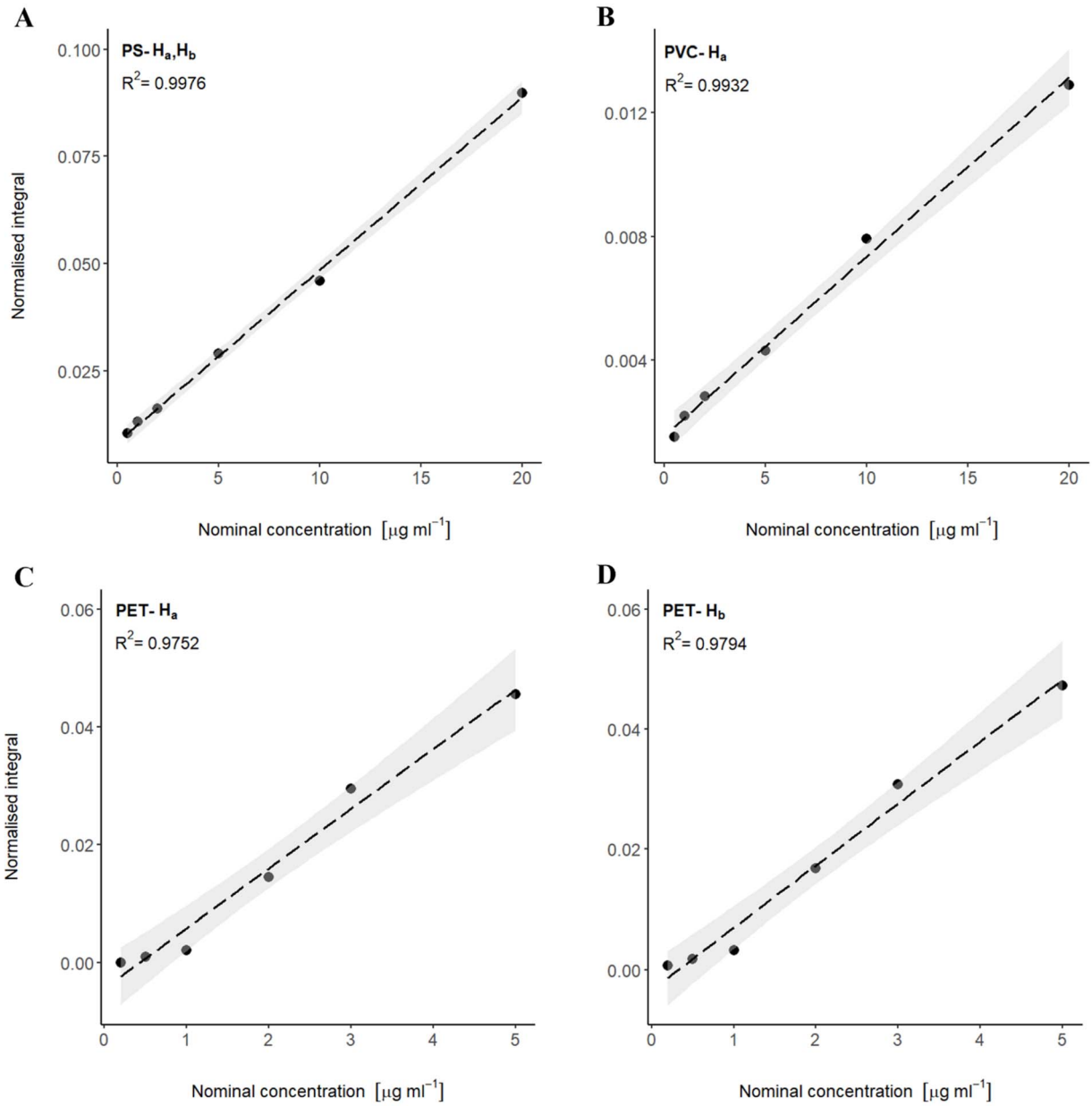

Fig. 5 Calibration graph of 24-day aged (A) PS-H_a,H_b and (B) PVC-H_a in THF-d_8 at a calibration range of 0.5–20 μg mL^{-1} and (C) PET-H_a and (D) PET-H_b in $CDCl_3$/TFA-d (4 : 1) at a calibration range of 0.2–5 μg mL^{-1}. Included is a confidence interval (0.95) and the coefficient of determination (R^2) for each MP.

emphasizing the improved analytical performance achieved here.

For PET, the lowest LOD was observed for the H_a signal at 0.87 μg mL^{-1}, while the highest LOQ was found for the H_b signal at 9.29 μg mL^{-1} (Table 2). These results fall within the range of previous reports[44] but show notable variability across literature. For example, a previous study reported LOD and LOQ values of 21 μg mL^{-1} and 81 μg mL^{-1}, respectively,[43] and later refined these values to 1 μg mL^{-1} and 4 μg mL^{-1}.[44] The PET values reported in this study are consistent with, or slightly higher than, the most sensitive prior assessments, demonstrating the robustness of the qNMR approach, even for aged and potentially degraded MP matrices.

Degradation products and environmental implications

Examining the full ^{1}H NMR spectra of artificially aged MPs, we observed additional small signals indicative of minor degradation products (Fig. 6), supported by 2D NMR analysis (Fig. S5 and S6 in the SI). In aged PS, notable spectral changes were observed at 8.01 ppm and 7.89 ppm (Fig. 6A), appearing as

Table 2 Calibration data of PS, PVC and PET after a 24-day aging process. Shown are the proton signals used, solvents, calibration ranges, coefficients of determination (R^2), limits of detection (LOD) and limits of quantification (LOQ) for each microplastic

Microplastic	PS	PVC	PET	
Proton signal	H_a,H_b	H_a	H_a	H_b
Solvent	THF-d_8	THF-d_8	$CDCl_3$/TFA-d (4 : 1)	
Calibration range [μg mL^{-1}]	0.5 to 20	0.5 to 20	0.2 to 5	0.2 to 5
Linearity R^2	0.9976	0.9932	0.9752	0.9794
LOD [μg mL^{-1}]	1.10	1.87	0.87	2.79
LOQ [μg mL^{-1}]	3.67	6.22	2.89	9.29

sharp, well-defined signals indicative of structural modifications associated with oxidative degradation, likely corresponding to the formation of oxidized monomers.[25,69] The signal at 8.01 ppm was likely attributable to benzylaldehyde, formed through oxidation or the formation of conjugated degradation products from the PS benzene ring. Similarly, the signal at 7.89 ppm likely corresponds to methyl benzoate, situated close to newly formed phenolic or carbonyl groups. These shifts are consistent with chemical modifications of the aromatic rings, such as the introduction of carbonyl (C=O) or hydroxyl (–OH) groups, resulting from photooxidative processes. Such transformations cause deshielding effects on the aromatic protons, shifting their resonances downfield compared to those of pristine PS.[70,71] These findings partially align with those of a previous study that detected both aromatic and aliphatic oxidized signals under more intense conditions (UV 750 W m^{-2}, 40 °C, 30 days) using ^{1}H NMR and TD-GC/MS.[53] The absence of aliphatic oxidation signals (2.3 to 5.0 ppm) in this study likely reflects the lower UV intensity and shorter exposure duration, highlighting the strong influence of aging conditions on the types of degradation products detected. These findings suggest that radical-induced oxidation at the aliphatic backbone also occurred, contributing to chain scission, although its spectral signatures were limited under the applied aging conditions. For PVC, well-resolved signals were observed between 5.0 and 11.0 ppm (Fig. 6B), consistent with the degradation processes such as dehydrochlorination and oxidation, which lead to the formation of a range of oxidized monomers, including unsaturated structures, aldehydes, ketones, and carboxylic acids.[72,73] Specifically, the signals at 10.82 ppm and 9.68 ppm correspond to aldehydic protons (–CHO groups), indicative of the formation of oxidation products, while the peak at 7.89 ppm is associated with vinylic protons from conjugated double bonds, a hallmark of dehydrochlorination and chain scission processes. The signal at 5.32 ppm likely corresponds to residual unsaturated structures formed during these degradation mechanisms, further confirming the oxidative transformations in PVC.[74] In contrast, aged PET showed minimal degradation in this study, with no degradation products detected (Fig. 6C). However, previous studies have shown that aged PET can exhibit small signals in the range of 0 to 4 ppm,[53] with intensity variations attributed to photo-induced modifications of its macromolecular structure.[26]

Additionally, the concentrations of the degradation products of both PS and PVC were quantified using the internal standard method, allowing for an assessment of chemical changes during aging. The results revealed a decrease in the concentrations of both degradation products from day 12 to day 24 of accelerated aging (Table 3). This trend suggests that, beyond the initial formation of oxidized structures, secondary degradation processes, such as chain scission or further oxidation, become more prominent with prolonged aging.[72,73] These secondary

Table 3 Quantification of degradation products of PS and PVC in THF-d_8 after 12 and 24 days of aging. Measured concentrations [μg mL^{-1}] were determined by the internal standard method with $DMSO_2$ as internal standard

MP degradation products	Signal [ppm]	Measured concentration [μg mL^{-1}]	
		12 d aged	24 d aged
PS	8.01	0.20	0.16
	7.89	0.18	0.14
PVC	10.82	8.85	8.26
	9.68	1.90	1.73
	7.89	0.60	0.51
	5.32	1.86	1.76

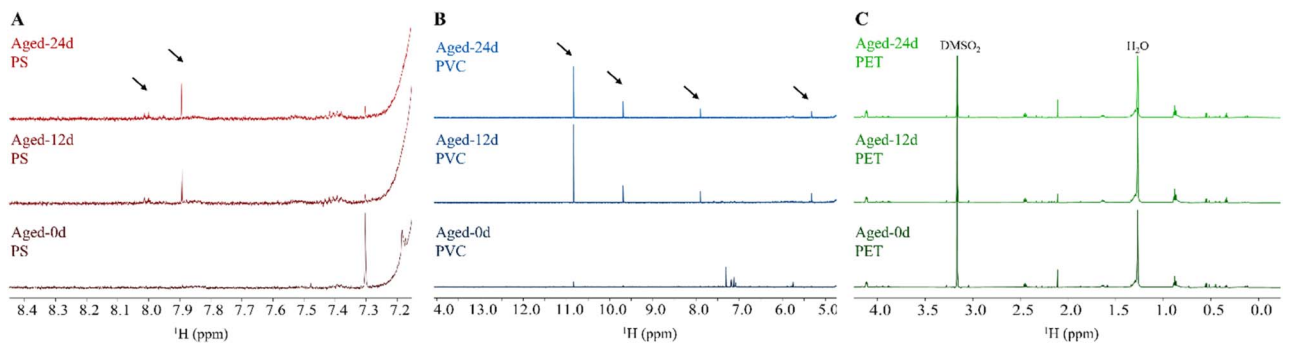

Fig. 6 Stackplots of ^{1}H NMR spectra of 0 day, 12 day and 24 day aged (A) PS and (B) PVC in THF-d_8, and (C) PET in $CDCl_3$/TFA-d (4 : 1). Arrows indicate signals attributed to degradation products formed during accelerated aging.

processes not only diminish the concentration of initially formed degradation products but also accelerate the breakdown of the MP matrix over time. Such findings highlight the dynamic nature of MP aging, where primary degradation products may undergo additional transformations, contributing to the ongoing degradation and potential embrittlement of the MP.[34,36] The presence of degradation products in environmental samples can overlap with MP signals, especially in the lower ppm range (<3 ppm), complicating MP quantification.[45,75] Careful sample preparation, including extraction and purification, is crucial to minimize spectral overlap with organic compounds, though this process is time-consuming and must be optimized to ensure accurate MP detection.[49,76–78] Additionally, the choice of internal standards may also pose difficulties, as some, like $DMSO_2$, could interfere with signals from unknown environmental compounds. In contrast, hexamethyl disiloxane (HMDSO), with a proton signal at 0.25 ppm [47] could be more suitable due to its minimal overlap potential.

Combining qNMR with FTIR and SEM for comprehensive analysis

The aging of MPs due to UV exposure and elevated temperatures significantly alters their chemical structure and physical properties, as shown by surface morphological changes (*e.g.*, SEM)[34,55,57] and chemical modifications (*e.g.*, FTIR).[62,64,66,79] These alterations present a challenge for both the detection and quantification of aged MPs and underscore the need for a multi-analytical approach to achieve a more comprehensive understanding. Importantly, MP degradation often occurs predominantly at the surface, while the bulk material remains less affected; thus, relying solely on FTIR may lead to an overestimation of the overall degradation degree. Therefore, the study demonstrated that by combining NMR spectroscopy with SEM and FTIR a comprehensive demonstration of MP aging can be achieved where complementary perspectives can be offered: SEM provides visual insights into surface degradation, FTIR identifies chemical changes and oxidation levels (*e.g.*, *via* the CI), and NMR enables molecular-level monitoring and quantification of MPs.[50]

^{1}H NMR spectroscopy is particularly useful for monitoring MP degradation, as aging can manifest in the spectra as new peaks, altered chemical shifts, peak broadening, and reduced signal intensity.[53,80] While no substantial peak shifts or broadening were observed in this study, as detailed in the previous section, distinct low-intensity signals corresponding to oxidized aromatic and unsaturated degradation byproducts were observed in aged PS and PVC samples, highlighting qNMR's unique capability to resolve molecular-level transformations that are not accessible through FTIR or SEM. The degradation-related changes depend on MP type, aging duration, and environmental conditions, factors that influence solubility and signal intensity, especially for environmentally realistic samples.[26,81,82] To ensure high-quality spectral data, qNMR was conducted at high MP concentrations, providing a detailed assessment of aged samples. Notably, the characteristic signals of aged MPs remained well-resolved, supporting the suitability of qNMR for quantification and suggesting that even at low MP concentrations,[46] effective analysis could still be performed. These findings indicate that, unlike FTIR, which may struggle to match aged MP spectra to reference libraries due to chemical changes, qNMR maintains its quantitative capacity despite MP aging.[83,84] Thus, NMR spectroscopy offers a valuable tool for assessing aged MPs, particularly in cases where FTIR sensitivity or library compatibility is limited.

Importantly, combining qNMR with FTIR and CI analysis not only strengthens structural and compositional assessments of MP aging but also highlights the value of integrating molecular spectroscopy techniques. Studies have shown that FTIR and solid-state ^{13}C NMR, for example, can yield differing results regarding oxidation markers like carboxyl content, underscoring the benefit of using multiple techniques in parallel.[85]

While this study demonstrates the complementarity of qNMR with FTIR and SEM, it was conducted under controlled laboratory conditions to determine whether aged MPs remain quantifiable at the molecular level. Identifying stable MP signals and emerging degradation products is essential groundwork for applying this integrated approach to real-world samples, where matrix interference and spectral overlap will present additional challenges. Prior studies on pristine MP mixtures support qNMR's potential,[49] and ongoing work now extends this to complex environmental matrices.

Conclusion

This study used NMR spectroscopy for MP quantification, with SEM and FTIR validating aging-related changes. Accelerated aging induced significant morphological and chemical changes in PS and PVC, with minimal alterations in PET. SEM showed surface degradation in PS and PVC, while FTIR confirmed oxidative degradation, reflected by increased carbonyl content in PS and PVC, and slight changes in PET.

Despite aging-induced changes, qNMR enabled reliable microplastic quantification, with relative errors between 1% to 18%. Key proton signals remained stable, allowing consistent integration across aging states. External calibration confirmed strong linearity ($R^2 > 0.975$), and low LOQ values (3.67–9.29 μg mL^{-1}) were achieved even after 24 days of aging, lower than those in previous pristine microplastic studies, highlighting qNMR's sensitivity and robustness. Minor ^{1}H NMR signals in aged PS and PVC (aromatic and aldehyde regions) indicated degradation byproducts, supporting qNMR's potential in early-stage degradation detection. These results underscore the strength of a multi-analytical approach, with qNMR proving a reliable, sensitive complement to SEM and FTIR for characterizing aged microplastics.

Author contributions

J. S. designed the methodology, conducted the investigation, curated and analyzed the data, and wrote the original draft. J. S., M. H., and W. W. reviewed and edited the manuscript. J. S. and M. H. contributed to visualization. W. W. administered the project and acquired funding.

Conflicts of interest

There are no conflicts to declare.

Data availability

The data supporting this article have been included as part of the SI.

The supplementary material contains the linearity data of the carbonyl index measurements of the aged MPs over time (Table S1); the full ^{1}H NMR spectra of 0 day, 12 day and 24 day aged PS and PVC in THF-d_8 (Fig. S1 and S2) and PET in $CDCl_3$/TFA-d (4 : 1) (Fig. S3); representative ^{1}H NMR spectra at the lowest and highest calibration concentrations used for LOD and LOQ determination (Fig. S4); and 2D NMR spectra (COSY, HSQC, HMBC) supporting the structural assignment of degradation products in 24 day aged PS and PVC (Fig. S5 and S6). See DOI: **https://doi.org/10.1039/d5em00393h**.

Acknowledgements

This research was financially supported by the Research Council of Norway (Grant No. 320456), the National Natural Science foundation of China (Grant No. 32061133005), and the Norwegian NMR Platform (NNP; Grant No. 226244/F50). SEM images were performed at ELMILAB at the University of Bergen. The authors would like to thank Jarl Underhaug (University of Bergen, Norway) for being available for consultation regarding the NMR data and Alessio Gomiero (NORCE, Norway) for his supply of some microplastic material. The authors used ChatGPT by OpenAI to rephrase and improve the language.

References

1 M. MacLeod, H. P. H. Arp, M. B. Tekman and A. Jahnke, The global threat from plastic pollution, *Science*, 2021, **373**, 61–65.
2 F. Wang, Q. Zhang, J. Cui, B. Bao, X. Deng, L. Liu, *et al.*, Polystyrene microplastics induce endoplasmic reticulum stress, apoptosis and inflammation by disrupting the gut microbiota in carp intestines, *Environ. Pollut.*, 2023, **323**, 121233.
3 A. L. Andrady and M. A. Neal, Applications and societal benefits of plastics, *Philos. Trans. R. Soc., B*, 2009, **364**, 1977–1984.
4 C. Arthur, H. Bamford and J. Baker, The Occurrence, Effects and Fate of Small Plastic Debris in the Oceans, *Proceedings of the International Research Workshop on the Occurrence, Effects and Fate of Microplastic Marine Debris*, Tacoma, WA, USA, 2008, pp. 9–11.
5 Y. Chae and Y. J. An, Effects of micro- and nanoplastics on aquatic ecosystems: Current research trends and perspectives, *Mar. Pollut. Bull.*, 2017, **124**, 624–632.
6 M. Cole and T. S. Galloway, Ingestion of Nanoplastics and Microplastics by Pacific Oyster Larvae, *Environ. Sci. Technol.*, 2015, **49**, 14625–14632.
7 S. Rist, A. Baun, R. Almeda and N. B. Hartmann, Ingestion and effects of micro- and nanoplastics in blue mussel (Mytilus edulis) larvae, *Mar. Pollut. Bull.*, 2019, **140**, 423–430.
8 GESAMP, *Proceedings of the GESAMP International Workshop on assessing the risks associated with plastics and microplastics in the marine environment*, UNESCO: United Nations Educational, Scientific and Cultural Organisation, 2020 [cited 2024 Feb 17], available from: **https://policycommons.net/artifacts/8220098/proceedings-of-the-gesamp-international-workshop-on-assessing-the-risks-associated-with-plastics-and-microplastics-in-the-marine-environment/9133791/**.
9 J. Boucher and G. Billard, *The Mediterranean: Mare Plasticum*, 2020.
10 D. K. A. Barnes, F. Galgani, R. C. Thompson and M. Barlaz, Accumulation and fragmentation of plastic debris in global environments, *Philos. Trans. R. Soc. London, Ser. B*, 2009, **364**, 1985–1998.
11 T. O'Brine and R. C. Thompson, Degradation of plastic carrier bags in the marine environment, *Mar. Pollut. Bull.*, 2010, **60**, 2279–2283.
12 M. A. Browne, A. Dissanayake, T. S. Galloway, D. M. Lowe and R. C. Thompson, Ingested microscopic plastic translocates to the circulatory system of the mussel, Mytilus edulis (L), *Environ. Sci. Technol.*, 2008, **42**, 5026–5031.
13 A. Lusher, Microplastics in the Marine Environment: Distribution, Interactions and Effects, in *Marine Anthropogenic Litter*, ed. M. Bergmann, L. Gutow and M. Klages, Springer International Publishing, Cham, 2015 [cited 2023 Jul 13], pp. 245–307, available from: **http://link.springer.com/10.1007/978-3-319-16510-3_10**.
14 S. Noventa, M. S. P. Boyles, A. Seifert, S. Belluco, A. S. Jiménez, H. J. Johnston, *et al.*, Paradigms to assess the human health risks of nano- and microplastics, *Microplast. Nanoplast.*, 2021, **1**, 9.
15 A. Rivaton and J. L. Gardette, Photo-oxidation of aromatic polymers, *Die Angewandte Makromolekulare Chemie*, 1998, **261–262**, 173–188.
16 A. L. Andrady, Microplastics in the marine environment, *Mar. Pollut. Bull.*, 2011, **62**, 1596–1605.
17 A. Jahnke, H. P. H. Arp, B. I. Escher, B. Gewert, E. Gorokhova, D. Kühnel, *et al.*, Reducing Uncertainty and Confronting Ignorance about the Possible Impacts of Weathering Plastic in the Marine Environment, *Environ. Sci. Technol. Lett.*, 2017, **4**, 85–90.
18 K. Wang, K. Wang, Y. Chen, S. Liang, C. Guo, W. Wang, *et al.*, Adsorption–desorption behavior of malachite green by potassium permanganate pre-oxidation polyvinyl chloride microplastics, *Environ. Technol. Innovation*, 2023, **30**, 103138.
19 C. Campanale, G. Dierkes, C. Massarelli, G. Bagnuolo and V. F. Uricchio, A Relevant Screening of Organic Contaminants Present on Freshwater and Pre-Production Microplastics, *Toxics*, 2020, **8**, 100.
20 C. Campanale, I. Savino, C. Massarelli and V. F. Uricchio, Assessment of metals associated with virgin pre-

production and freshwater microplastics collected by an Italian river, *NanoImpact*, 2022, **28**, 100438.

21 I. Savino, C. Campanale, P. Trotti, C. Massarelli, G. Corriero and V. F. Uricchio, Effects and Impacts of Different Oxidative Digestion Treatments on Virgin and Aged Microplastic Particles, *Polymers*, 2022, **14**, 1958.

22 L. Hermabessiere, A. Dehaut, I. Paul-Pont, C. Lacroix, R. Jezequel, P. Soudant, *et al.*, Occurrence and effects of plastic additives on marine environments and organisms: A review, *Chemosphere*, 2017, **182**, 781–793.

23 G. L. Wei, D. Q. Li, M. N. Zhuo, Y. S. Liao, Z. Y. Xie, T. L. Guo, *et al.*, Organophosphorus flame retardants and plasticizers: Sources, occurrence, toxicity and human exposure, *Environ. Pollut.*, 2015, **196**, 29–46.

24 H. Jiang, J. Bu, K. Bian, J. Su, Z. Wang, H. Sun, *et al.*, Surface change of microplastics in aquatic environment and the removal by froth flotation assisted with cationic and anionic surfactants, *Water Res.*, 2023, **233**, 119794.

25 P. Liu, X. Zhan, X. Wu, J. Li, H. Wang and S. Gao, Effect of weathering on environmental behavior of microplastics: Properties, sorption and potential risks, *Chemosphere*, 2020, **242**, 125193.

26 K. Zhang, A. H. Hamidian, A. Tubić, Y. Zhang, J. K. H. Fang, C. Wu, *et al.*, Understanding plastic degradation and microplastic formation in the environment: A review, *Environ. Pollut.*, 2021, **274**, 116554.

27 H. Jiang, Y. Zhang, K. Bian, C. Wang, X. Xie, H. Wang, *et al.*, Is it possible to efficiently and sustainably remove microplastics from sediments using froth flotation?, *Chem. Eng. J.*, 2022, **448**, 137692.

28 J. N. Hanun, F. Hassan and J. J. Jiang, Occurrence, fate, and sorption behavior of contaminants of emerging concern to microplastics: Influence of the weathering/aging process, *J. Environ. Chem. Eng.*, 2021, **9**, 106290.

29 W. Wang, J. Ge and X. Yu, Bioavailability and toxicity of microplastics to fish species: A review, *Ecotoxicol. Environ. Saf.*, 2020, **189**, 109913.

30 J. Lei, Q. Ma, X. Ding, Y. Pang, Q. Liu, J. Wu, *et al.*, Microplastic environmental behavior and health risk assessment: a review, *Environ. Chem. Lett.*, 2024, **22**, 2913–2941.

31 N. Cingotti, G. K. Jensen and Health and Environment Alliance (HEAL), *Food Contact Materials and Chemical Contamination*, Health and Environment Alliance, Brussels, Belgium, 2019.

32 C. Campanale, C. Massarelli, I. Savino, V. Locaputo and V. F. Uricchio, A Detailed Review Study on Potential Effects of Microplastics and Additives of Concern on Human Health, *Int. J. Environ. Res. Public Health*, 2020, **17**, 1212.

33 A. L. Andrady, Persistence of Plastic Litter in the Oceans, in *Marine Anthropogenic Litter*, ed. M. Bergmann, L. Gutow and M. Klages, Springer International Publishing, Cham, 2015 [cited 2024 Dec 5], pp. 57–72, DOI: **10.1007/978-3-319-16510-3_3**.

34 B. Gewert, M. M. Plassmann and M. MacLeod, Pathways for degradation of plastic polymers floating in the marine environment, *Environ. Sci.: Processes Impacts*, 2015, **17**, 1513–1521.

35 M. Gardette, A. Perthue, J. L. Gardette, T. Janecska, E. Földes, B. Pukánszky, *et al.*, Photo- and thermal-oxidation of polyethylene: Comparison of mechanisms and influence of unsaturation content, *Polym. Degrad. Stab.*, 2013, **98**, 2383–2390.

36 B. Singh and N. Sharma, Mechanistic implications of plastic degradation, *Polym. Degrad. Stab.*, 2008, **93**, 561–584.

37 R. Mao, M. Lang, X. Yu, R. Wu, X. Yang and X. Guo, Aging mechanism of microplastics with UV irradiation and its effects on the adsorption of heavy metals, *J. Hazard. Mater.*, 2020, **393**, 122515.

38 C. D. Rummel, M. G. J. Löder, N. F. Fricke, T. Lang, E. M. Griebeler, M. Janke, *et al.*, Plastic ingestion by pelagic and demersal fish from the North Sea and Baltic Sea, *Mar. Pollut. Bull.*, 2016, **102**, 134–141.

39 L. Shen, Y. Wang, R. Liu, Y. Yang, Y. Liu and B. Xing, Aging characteristics of degradable and non-biodegradable microplastics and their adsorption mechanism for sulfonamides, *Sci. Total Environ.*, 2023, **901**, 166452.

40 J. Brandon, M. Goldstein and M. D. Ohman, Long-term aging and degradation of microplastic particles: Comparing in situ oceanic and experimental weathering patterns, *Mar. Pollut. Bull.*, 2016, **110**, 299–308.

41 S. Veerasingam, M. Ranjani, R. Venkatachalapathy, A. Bagaev, V. Mukhanov, D. Litvinyuk, *et al.*, Contributions of Fourier transform infrared spectroscopy in microplastic pollution research: A review, *Crit. Rev. Environ. Sci. Technol.*, 2021, **51**, 2681–2743.

42 J. Almond, P. Sugumaar, M. N. Wenzel, G. Hill and C. Wallis, Determination of the carbonyl index of polyethylene and polypropylene using specified area under band methodology with ATR-FTIR spectroscopy, *e-Polym.*, 2020, **20**, 369–381.

43 N. Peez, M. C. Janiska and W. Imhof, The first application of quantitative 1H NMR spectroscopy as a simple and fast method of identification and quantification of microplastic particles (PE, PET, and PS), *Anal. Bioanal. Chem.*, 2019, **411**, 823–833.

44 N. Peez and W. Imhof, Quantitative 1 H-NMR spectroscopy as an efficient method for identification and quantification of PVC, ABS and PA microparticles, *Analyst*, 2020, **145**, 5363–5371.

45 N. Peez, J. Becker, S. M. Ehlers, M. Fritz, C. B. Fischer, J. H. E. Koop, *et al.*, Quantitative analysis of PET microplastics in environmental model samples using quantitative 1H-NMR spectroscopy: validation of an optimized and consistent sample clean-up method, *Anal. Bioanal. Chem.*, 2019, **411**, 7409–7418.

46 J. Schmidt, M. Haave, J. Underhaug and W. Wang, Unlocking the potential of NMR spectroscopy for precise and efficient quantification of microplastics, *Microplast. Nanoplast.*, 2024, **4**, 17.

47 M. Günther and W. Imhof, Highly selective solid–liquid extraction of microplastic mixtures as a pre-preparation

tool for quantitative nuclear magnetic resonance spectroscopy studies, *Analyst*, 2024, **149**, 5800–5811.
48 M. Günther and W. Imhof, Simultaneous quantification of microplastic particles by non-deuterated (NoD) 1 H-qNMR from samples comprising different polymer types, *Analyst*, 2023, **148**, 1151–1161.
49 J. Schmidt, M. Haave and W. Wang, Applicability of NMR spectroscopy to quantify microplastics across varying concentrations in polymer mixtures, *RSC Adv.*, 2025, **15**, 13041–13052.
50 A. Corti, V. Vinciguerra, V. Iannilli, L. Pietrelli, A. Manariti, S. Bianchi, *et al.*, Thorough Multianalytical Characterization and Quantification of Micro- and Nanoplastics from Bracciano Lake's Sediments, *Sustainability*, 2020, **12**, 878.
51 N. Peez, T. Rinesch, J. Kolz and W. Imhof, Applicable and cost-efficient microplastic analysis by quantitative 1H-NMR spectroscopy using benchtop NMR and NoD methods, *Magn. Reson. Chem.*, 2022, **60**, 172–183.
52 A. Mauel, B. Pötzschner, N. Meides, R. Siegel, P. Strohriegl and J. Senker, Quantification of photooxidative defects in weathered microplastics using 13 C multiCP NMR spectroscopy, *RSC Adv.*, 2022, **12**, 10875–10885.
53 G. Giaganini, M. Cifelli, D. Biagini, S. Ghimenti, A. Corti, V. Castelvetro, *et al.*, Multi-Analytical Approach to Characterize the Degradation of Different Types of Microplastics: Identification and Quantification of Released Organic Compounds, *Molecules*, 2023, **28**, 1382.
54 G. F. Pauli, B. U. Jaki and D. C. Lankin, Quantitative ^{1} H NMR: Development and Potential of a Method for Natural Products Analysis, *J. Nat. Prod.*, 2005, **68**, 133–149.
55 X. D. Xue, C. R. Fang and H. F. Zhuang, Adsorption behaviors of the pristine and aged thermoplastic polyurethane microplastics in Cu(II)-OTC coexisting system, *J. Hazard. Mater.*, 2021, **407**, 124835.
56 C. Chen, F. Wei, L. Ye, Y. Wang, L. Long, C. Xu, *et al.*, Adsorption of Cu2+ by UV aged polystyrene in aqueous solution, *Ecotoxicol. Environ. Saf.*, 2022, **232**, 113292.
57 K. Wang, Y. Kou, C. Guo, K. Wang, J. Li, J. Schmidt, *et al.*, Comparison of rhodamine B adsorption and desorption on the aged non-degradable and degradable microplastics: Effects of charge-assisted hydrogen bond and underline mechanism, *Environ. Technol. Innovation*, 2024, **35**, 103739.
58 T. Hüffer, A. K. Weniger and T. Hofmann, Sorption of organic compounds by aged polystyrene microplastic particles, *Environ. Pollut.*, 2018, **236**, 218–225.
59 C. C. Tang, H. I. Chen, P. Brimblecombe and C. L. Lee, Textural, surface and chemical properties of polyvinyl chloride particles degraded in a simulated environment, *Mar. Pollut. Bull.*, 2018, **133**, 392–401.
60 R. Guo, E. Yu, J. Liu and Z. Wei, Agitating transformation during vinyl chloride suspension polymerization: aggregation morphology and PVC properties, *RSC Adv.*, 2017, **7**, 24022–24029.
61 C. Ioakeimidis, K. N. Fotopoulou, H. K. Karapanagioti, M. Geraga, C. Zeri, E. Papathanassiou, *et al.*, The degradation potential of PET bottles in the marine environment: An ATR-FTIR based approach, *Sci. Rep.*, 2016, **6**, 23501.
62 C. Campanale, I. Savino, C. Massarelli and V. F. Uricchio, Fourier Transform Infrared Spectroscopy to Assess the Degree of Alteration of Artificially Aged and Environmentally Weathered Microplastics, *Polymers*, 2023, **15**, 911.
63 S. Klempová, M. Oravec and K. Vizárová, Analysis of thermally and UV–Vis aged plasticized PVC using UV–Vis, ATR-FTIR and Raman spectroscopy, *Spectrochim. Acta, Part A*, 2023, **294**, 122541.
64 K. Wang, K. Wang, S. Liang, C. Guo, W. Wang and J. Wang, Accelerated aging of polyvinyl chloride microplastics by UV irradiation: Aging characteristics, filtrate analysis, and adsorption behavior, *Environ. Technol. Innovation*, 2023, **32**, 103405.
65 J. Yu, L. Sun, C. Ma, Y. Qiao and H. Yao, Thermal degradation of PVC: A review, *Waste Manage.*, 2016, **48**, 300–314.
66 A. P. D. S. Pereira, M. H. P. D. Silva, É. P. Lima Júnior, A. D. S. Paula and F. J. Tommasini, Processing and Characterization of PET Composites Reinforced With Geopolymer Concrete Waste, *Mater. Res.*, 2017, **20**, 411–420.
67 T. Sang, C. J. Wallis, G. Hill and G. J. P. Britovsek, Polyethylene terephthalate degradation under natural and accelerated weathering conditions, *Eur. Polym. J.*, 2020, **136**, 109873.
68 Y. Xu, R. Cui, Y. Han, J. Jiang, D. Hu, L. Zhao, *et al.*, Efficient Alcoholysis of Poly(ethylene terephthalate) by Using Supercritical Carbon Dioxide as a Green Solvent, *Polymers*, 2024, **16**, 1564.
69 X. Zhang, M. Peng, Q. Zhang, X. Ma, J. Song, M. Sun, *et al.*, UV-photoaging behavior of polystyrene microplastics enhanced by thermally-activated persulfate, *J. Environ. Chem. Eng.*, 2023, **11**, 110508.
70 E. Yousif and R. Haddad, Photodegradation and photostabilization of polymers, especially polystyrene: review, *SpringerPlus*, 2013, **2**, 398.
71 A. Torikai and H. Shibata, Photodegradation of Polystyrene: Effect of Polymer Structure on the Formation of Degradation Products, *Arabian J. Sci. Eng.*, 2002, **27**, 11–24.
72 Z. Ouyang, Z. Zhang, Y. Jing, L. Bai, M. Zhao, X. Hao, *et al.*, The photo-aging of polyvinyl chloride microplastics under different UV irradiations, *Gondwana Res.*, 2022, **108**, 72–80.
73 A. Marongiu, T. Faravelli, G. Bozzano, M. Dente and E. Ranzi, Thermal degradation of poly(vinyl chloride), *J. Anal. Appl. Pyrolysis*, 2003, **70**, 519–553.
74 E. Yousif and A. Hasan, Photostabilization of poly(vinyl chloride) – Still on the run, *J. Taibah Univ. Sci.*, 2015, **9**, 421–448.
75 S. Zhao, L. Zhu, L. Gao and D. Li, Chapter 2 - Limitations for Microplastic Quantification in the Ocean and Recommendations for Improvement and Standardization, in *Microplastic Contamination in Aquatic Environments*, ed. E. Y. Zeng, Elsevier, 2018 [cited 2025 Apr 25], pp. 27–49, available from: **https://www.sciencedirect.com/science/article/pii/B9780128137475000023**.

76 M. Rani, S. Ducoli, L. E. Depero, M. Prica, A. Tubić, Z. Ademovic, *et al.*, A Complete Guide to Extraction Methods of Microplastics from Complex Environmental Matrices, *Molecules*, 2023, **28**, 5710.

77 A. L. Lusher, K. Munno, L. Hermabessiere and S. Carr, Isolation and Extraction of Microplastics from Environmental Samples: An Evaluation of Practical Approaches and Recommendations for Further Harmonization, *Appl. Spectrosc.*, 2020, **74**, 1049–1065.

78 M. G. J. Löder, H. K. Imhof, M. Ladehoff, L. A. Löschel, C. Lorenz, S. Mintenig, *et al.*, Enzymatic Purification of Microplastics in Environmental Samples, *Environ. Sci. Technol.*, 2017, **51**, 14283–14292.

79 A. Käppler, D. Fischer, S. Oberbeckmann, G. Schernewski, M. Labrenz, K. J. Eichhorn, *et al.*, Analysis of environmental microplastics by vibrational microspectroscopy: FTIR, Raman or both?, *Anal. Bioanal. Chem.*, 2016, **408**, 8377–8391.

80 T. M. Alam, M. Celina, R. A. Assink, R. L. Clough, K. T. Gillen and D. R. Wheeler, Investigation of Oxidative Degradation in Polymers Using 17O NMR Spectroscopy, *Macromolecules*, 2000, **33**, 1181–1190.

81 X. Xu, S. Wang, F. Gao, J. Li, L. Zheng, C. Sun, *et al.*, Marine microplastic-associated bacterial community succession in response to geography, exposure time, and plastic type in China's coastal seawaters, *Mar. Pollut. Bull.*, 2019, **145**, 278–286.

82 A. Käppler, M. Fischer, B. M. Scholz-Böttcher, S. Oberbeckmann, M. Labrenz, D. Fischer, *et al.*, Comparison of μ-ATR-FTIR spectroscopy and py-GCMS as identification tools for microplastic particles and fibers isolated from river sediments, *Anal. Bioanal. Chem.*, 2018, **410**, 5313–5327.

83 Y. Shi, L. Shi, H. Huang, K. Ye, L. Yang, Z. Wang, *et al.*, Analysis of aged microplastics: a review, *Environ. Chem. Lett.*, 2024, **22**, 1861–1888.

84 G. Renner, T. C. Schmidt and J. Schram, A New Chemometric Approach for Automatic Identification of Microplastics from Environmental Compartments Based on FT-IR Spectroscopy, *Anal. Chem.*, 2017, **89**, 12045–12053.

85 T. Menzel, N. Meides, A. Mauel, U. Mansfeld, W. Kretschmer, M. Kuhn, *et al.*, Degradation of low-density polyethylene to nanoplastic particles by accelerated weathering, *Sci. Total Environ.*, 2022, **826**, 154035.

